Düzce Üniversitesi Orman Fakültesi Ormancılık Dergisi
e-ISSN: 2148-7855

TYPE Research Article
PUBLISHED 30 December 2025
DOI 10.58816/duzceod/1675848

# Object-Based Image Classification Process at Landscape Level Based on Spectral Index Extraction Using Sentinel 2 MSI Satellite Imagery

Esin Karamanlı*[1] & Ömer Faruk Uzun[2]

[1] Çukurova Üniversitesi, Mimarlık Fakültesi, Peyzaj Mimarlığı Bölümü, Adana, Türkiye.
[2] Sakarya Uygulamalı Bilimler Üniversitesi, Ziraat Fakültesi, Peyzaj Mimarlığı Bölümü, Sakarya, Türkiye.

OPEN ACCESS

*CORRESPONDING AUTHOR
Esin KARAMANLI
esin.karamanli@gmail.com

RECEIVED 14 April 2025
ACCEPTED 30 November 2025

CITATION
Karamanlı, E., & Uzun, Ö. F. (2025). Object-based image classification process at landscape level based on spectral index extraction using Sentinel 2 MSI satellite imagery. *Düzce Üniversitesi Orman Fakültesi Ormancılık Dergisi, 21*(2), 66–81. https://doi.org/10.58816/duzceod.1675848



Land Cover-Land Use (LC/LU) classification provides data for effective management of environmental and ecological decisions at the landscape scale. In this process, Sentinel-2 Multi Spectral Imager (MSI) satellite images contribute to classification methods by facilitating information extraction with their high spectral resolution. While index-based methods mostly focus on the separation of single classes, landscapes require the separation of multiple classes. This study shows how different spectral indexes derived from Sentinel-2 MSI imagery can be used in large areas with the object-based image classification technique. The Silifke district of Mersin province was selected as a sample area. Normalized Difference Vegetation Index (NDVI), Normalized Difference Water Index (NDWI), Built-up Area Extraction Index (BAEI), Built-up Area Index (BAI), Band Ratio (BR28, BR38), Normalized Built-up Area Index (NBAI), New Building Index (NBI), Urban Index (UI), Normalized Difference Soil Tillage Index (NDTI), Red Edge Based Normalized Difference Vegetation Index (NDVIre) and Normalized Difference Water Index (MNDWI) were used. While no significant results were obtained with BR28, BR38, NBAI, NBI and UI, 0.8815 kappa coefficient of 0.8815 and overall accuracy rate of %94.11 were obtained with other indexes.

KEYWORDS
object-based image analysis, spectral indexes, classification, nearest neighbour algorithm, machine learning

## Sentinel 2 MSI Uydu Görüntülerini Kullanarak Spektral İndeks Çıkarımına Dayalı Peyzaj Düzeyinde Nesne Tabanlı Görüntü Sınıflandırma Süreci

Arazi Örtüsü-Arazi Kullanımı (AÖ-AK) sınıflandırması, peyzaj ölçeğinde çevresel ve ekolojik kararların etkin şekilde yönetilmesi için veriler sunar. Bu süreçte, Sentinel-2 Multispektral Görüntüleyici (MSI) uydu görüntüleri, yüksek spektral çözünürlükleriyle bilgi çıkarımını kolaylaştırarak sınıflandırma yöntemlerine katkı sağlar. İndeks tabanlı yöntemler çoğunlukla tek sınıf ayrımına odaklanırken, peyzajlarda çoklu sınıfların ayrıştırılması gerekmektedir. Bu çalışmada, Sentinel-2 MSI görüntülerinden türetilen çeşitli spektral indekslerin nesne tabanlı görüntü sınıflandırma tekniği ile geniş alanlarda nasıl kullanılabileceği ortaya konulmuştur. Örneklem alanı olarak Mersin ili Silifke ilçesi seçilmiştir. Normalize Edilmiş Fark Vejetasyon İndeksi (NDVI), Normalize Edilmiş Fark Su İndeksi (NDWI), Yapı Alanı Çıkarım İndeksi (BAEI), Yapı Alan İndeksi (BAI), Bant Oranı (BR28, BR38), Normalize Edilmiş Yapı Alan İndeksi (NBAI), Yeni Yapı İndeksi (NBI), Kent İndeksi (UI), Normalize Edilmiş Fark Toprak İşleme İndeksi (NDTI), Kırmızı Kenar Bazlı Normalize Edilmiş Fark Vejetasyon İndeksi (NDVIre) ve Dönüştürülmüş Normalize Fark Su İndeksi (MNDWI) kullanılmıştır. BR28, BR38, NBAI, NBI ve UI ile anlamlı sonuçlar elde edilemezken, diğer indekslerle 0,8815 kappa katsayısı ve %94,11 genel doğruluk oranı sağlanmıştır.

ANAHTAR KELİMELER
nesne-tabanlı görüntü analizi, spektral indisler, sınıflandırma, en yakın komşu algoritması, makine öğrenmesi

## 1. INTRODUCTION

Recent developments in digital image processing have helped the development of several techniques that facilitate the conversion of data sets obtained via various satellite platforms into land cover-land use (LC/LU) maps (Bayburt, 2009; Kalkan & Maktav, 2010). One of the most fundamental steps in digital image processing is image classification techniques (Jawak et al., 2015). The evolution of these techniques, alongside advances in machine learning algorithms, initially relied on pixel-based methods. However, in recent years, the proliferation of satellite platforms providing high-resolution spatial and spectral data—now publicly accessible—has significantly boosted the adoption of object-based classification approaches (Bhaskaran et al., 2010).

Object-based programming is an information-extracting approach that allows the use of multi-information, such as shape, texture, area, and topological relations with other (neighbour) objects, in addition to spectral information obtained from objects and used for image classification (Torres-Sanchez et al., 2015). In most existing approaches, the spectral information in the remote sensing bands is pixel-based, as it consists of the electromagnetic reflectance value reflecting the physical characteristic of the ground, enables the creation of land cover/use maps using only multiband spectral data (Bayburt, 2009; Nandam & Patel, 2021). However, in the recent years, it has been seen that object-based classification methods provide results with higher accuracy according to pixel-based ones (Duro et al., 2012; Flanders et al., 2003; Kalkan & Maktav, 2010; Rastner et al., 2014). For example, Tehrany et al. (2014) used DEM ancillary data with Nearest Neighbour (NN) algorithm, Whiteside et al. (2011) used Digital Elevation Model (DEM) and surface contours ancillary data with Weighted Scoring Model (WSM), Newman et al. (2011) used Digital Surface Model (DSM) and road networks ancillary data with NN algorithm, Myint et al. (2011), Ouchra et al. (2022), and Tehrany et al. (2014) used DEM ancillary data with NN algorithm by comparing to other pixel-based classification methods. In their studies, it was shown that object-based classification results provided higher accuracy scores.

Based on the insights gained from these studies, detailed object-based image analysis (OBIA), which dates back to the 1970s (Blaschke, 2010), involves extracting homogeneous image objects (segments) at a specified resolution (Flanders et al., 2003) and subsequently assigning them to relevant object classes. Instead of using pixels in their raw form, they are transformed into information that defines objects (classes), making them easier to separate (Bayburt, 2009; Blaschke, 2010). In the field of remote sensing, numerous efforts have been made to develop effective approaches for information extraction processes (Jawak et al., 2015). At this stage, easy access to high-resolution satellite images provides an advantage for more precise information extraction through the development of advanced classification schemes. One of the most effective methods for meaningful extraction of spectral information from object-based segmented images is assumed to be the index-based classification approach (Bhatt et al., 2018; Magpantay et al., 2019). In this approach, auxiliary factors that help determine a class are spectral thresholds, which enable the extraction of information within maximum and minimum ranges.

The Normalized Difference Vegetation Index (NDVI) developed by Rouse et al. (1973) allows vegetation to be easily separated from other classes (Nandam & Patel, 2021). NDVI has become the pioneer of many other spectral reflectance-based indexes. The Normalized Difference Water Index (NDWI), developed by McFeeters (1996), and the Urban Index (UI), developed by Kawamura et al. (1996), have been used in many studies to classify land use/land cover at the landscape level (Kebede et al., 2022; Zha et al., 2003) and have contributed to the development of many other indexes created for similar purposes. These indexes, developed with the introduction of Landsat satellite imagery since 1972, have been used in many classification studies based on index-based thresholding, yielding meaningful results (Harrak et al., 2025). For example, Magpantay et al. (2019) classified water, built-up, and vegetation areas using NDVI, NDWI, and Normalized Difference Built-

up Index (NDBI) with Landsat 8 OLI imagery. Similarly, Zha et al. (2003) extracted built-up areas using the NDBI index with Landsat TM imagery. Lemenkova & Debeir (2023) focused on green surface extraction using the Vegetation Index (VI) with Landsat 8–9 OLI/TIRS imagery. Additionally, Da Silva et al. (2020) classified forest, agricultural, built-up, and water surfaces using NDVI, Soil-Adjusted Vegetation Index (SAVI), Leaf Area Index (LAI), Enhanced Vegetation Index (EVI), and NDWI with Landsat 8 OLI imagery. The common resolution of these studies was 30 meters.

In many studies comparing Sentinel 2 MSI (its the short revisit time (5 days) and 10-meter spatial resolution) and Landsat 7-8-9 images, it has been seen that band combinations prepared with Sentinel 2 MSI band collections put forward results with higher accuracy (Esetlili et al., 2018; Karakus et al., 2017; Nwagoum et al., 2023). Although many attempts have been made to combine and compare both band groups (Kebede et al., 2022; Zhang et al., 2023), it should be noted that studies focusing on index-based classification of Sentinel-2 MSI imagery typically target only one or a limited number of land cover or land use classes. For example, Kebede et al. (2022) provided the extraction of impervious surfaces with Built-up Area Extraction Index (BAEI), Band Ratio for Built-up Area (BRBA), Modified Built-up Index (MBI), Normalized Built-up Area Index (NBAI), New Built- up Index (NBI), NDBI, and UI, Osgouei et al. (2019) obtained built-up areas with Normalized Difference Tillage Index (NDTI), Red-Edge-Based Normalized Vegetation Index (NDVIre), and Modified Normalized Difference Water Index (MNDWI), Rouibah (2023) obtained built-up areas with the Blue-Near-Infrared (BR28) and the Green-Near-Infrared (BR38) Bands Ratio (BR38), and Du et al. (2016) obtained water surfaces with MNDWI index by using Sentinel 2A MSI imagery.

This study presents a comprehensive object-based image analysis (OBIA) approach that integrates multiple spectral index layers derived from Sentinel-2 MSI imagery to perform land use/land cover (LU/LC) classification at the landscape scale. Unlike most previous studies that focus on a single class or a limited number of classes, this research emphasizes the multi-class separation required for complex and heterogeneous landscapes. The proposed method not only utilizes spectral thresholds for index-based classification but also incorporates ancillary data to enhance accuracy in distinguishing spectrally similar classes. By applying this integrated approach in the Silifke district of Türkiye, the study aims to demonstrate the reliability, adaptability, and scalability of index-based OBIA methods in generating high-resolution LU/LC maps suitable for planning and environmental monitoring purposes.

## 2. MATERIAL AND METHOD

### 2.1. Material

#### *2.1.1. Study Area*

Silifke district, which is 85 km away from Mersin city center, and 73 km away from Mut district center, is located between $37^0$26′39″ - $36^0$14′5.48″ north-south latitude and $33^0$49′36.98″- $33^0$35′38.94″ east-west longitude. Silifke, which is surrounded by Erdemli in the west, and by Mut and Gülnar district in the east, has typical Mediterranean climate characteristics. The district located at an altitude of 30 meters includes 88 neighbourhoods within its boundaries. Its surface area is 2590 $km^2$ (TÜİK, 2023). Figure 1 shows the location of the study area within global boundaries.

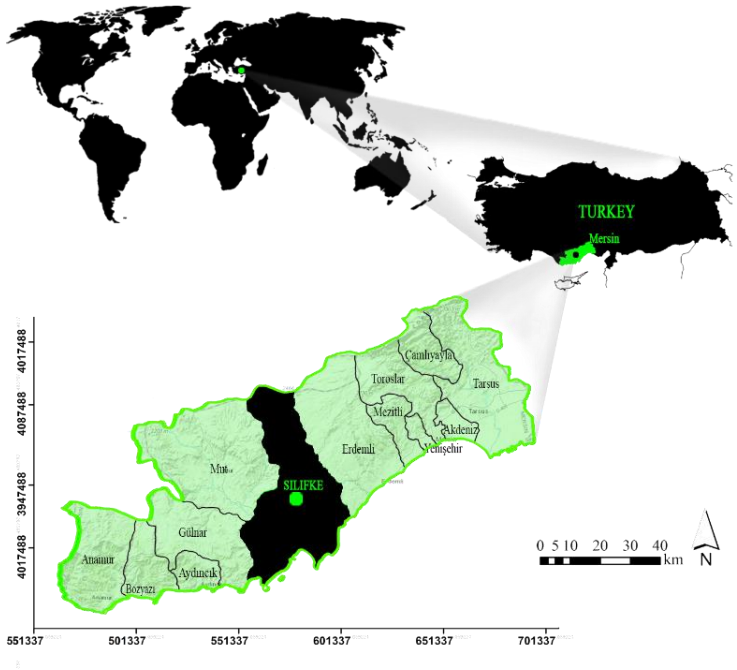


**Figure 1.** *The Silifke district sample area*

### *2.1.2. Data Set and Acquisition Source*

Sentinel 2B MSI data for the study area were captured on 21 July 2024 providing 13 spectral bands: four bands at 10-meter resolution, six bands at 20-meter resolution, and three bands at 60-meter resolution (NASA, 2025). The primary dataset of the study is the standard Sentinel-2 Level-1C product, produced by radiometric and geometric corrections (Sentiwiki, 2025), including ortho-rectification and spatial registration on a global system with sub-pixel accuracy (Du et al., 2016). Therefore, geometric, and radiometric corrections were not required for this dataset. While extracting information from the prepared index images using the primary dataset, ancillary dataset (DEM and stand map) was used in cases where spectral segregation for different classes became difficult and complex (Table 1).

**Table 1.** *Dataset used in the OBIA for LC/LU classification*

| **Primary Data Set:** Sentinel 2B_MSIL1C_20240721T082609_N0510_R021_T36SWF_20240721T10141 | | | |
|---|---|---|---|
| **Name** | **Description** | **Resolution** | **Reference** |
| B02 | Blue, 492.4 nm (S2A), 492.1 nm (S2B) | 10 m | (CB, 2024) |
| B03 | Green, 559.8 nm (S2A), 559.0nm (S2B) | 10 m | |
| B04 | Red, 664.6 nm (S2A), 665.0 nm (S2B) | 10 m | |
| B07 | Veg. Red Edge, 782.8 nm (S2A), 779.7 nm | 20 m | |
| B08 | NIR, 832.8 nm (S2A), 833.0 nm (S2B) | 10 m | |
| B11 | SWIR, 1613.7 nm (S2A), 1610.4 nm (S2B) | 20 m | |
| B12 | SWIR, 2202.4 nm (S2A), 2185.7 nm (S2B) | 20 m | |
| **Ancillary Data Set** | | | |
| DEM (Digital Elevation Model) | | Resampled | (Özgür, 2023) |
| Stand Map | | Digitalized | (OGM, 2021) |

## 2.2. Method

### *2.2.1. Image Pre-Processing*

The only pre-processing step required before preparing the index layers is the downscaling process to ensure Sentinel 2 MSI bands with identical spatial resolution (10 m for this study). Downscaling is defined as the restoration of fine-scale values to a specified scale, assuming that they are

descriptive of coarse scale values (Hong et al., 2011). This process is also called the reduction of coarse resolution data (dependent variable) to fine resolution using the available information (independent variable set) at the desired resolution.

The widespread use of machine learning algorithms for geostatistical applications has led to the improvement of estimation performances that show spatial dependence among satellite band groups and has caused an increase in the success rates of downscaling operations. Therefore, downscaling operations were performed for Sentinel 2 MSI bads using Random Forest (RF), Support Vector Machine (SVM), and Artificial Neural Network (ANN) machine learning algorithms. While the B02, B03, B04, and B08 bands with 10 m spatial resolution were evaluated as independent variable sets, the B07, B11, and B12 bands with 20 m spatial resolution were accepted as dependent variables separately and the operations were carried out.

*2.2.2. Image Segmentation*

One of the most important steps for ensuring object-based classification study with high accuracy scores is the segmentation process. At this stage, the image to be segmented was chosen as Sentinel 2 MSI natural colour band combination, which is the same way the human eye perceives the world (uses red (B04), green (B03), and blue (B02) channels), as given in Figure 2.

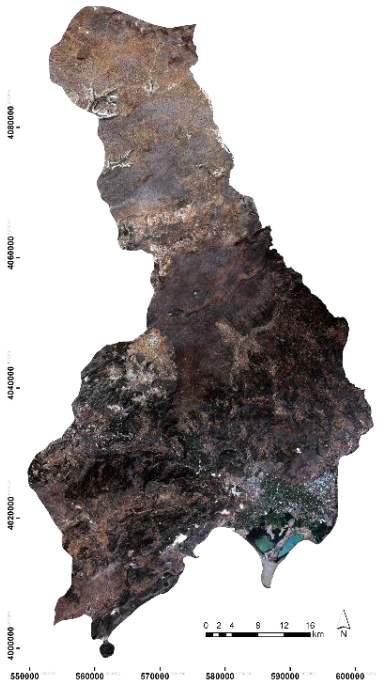


**Figure 2.** *Natural band (4,3,2) composite of the Silifke district*

The image was firstly segmented using the multiresolution segmentation algorithm in eCognition Developer 64 software. The algorithm is primarily an iterative bottom-up segmentation method starting with individual pixels and merging these pixels based on pixel heterogeneity (Trimble, 2025). The segmentation of the images was prepared by three parameters: scale, shape, and compactness. In here, scale parameter is a value that affects the heterogeneity of objects occurring in different sizes on the satellite image (Nussbaum & Menz, 2008). As the scale parameter increases, the image is divided into fewer segments, and result in segments consisting of a mixture of different land use types. When the scale parameter is too small, objects are divided into more segments than necessary. Shape parameter is based on the standard deviation of the spectral colours. Compactness gives a relative weighting against smoothness. In line with this information, the natural colour composite image was segmented using different parameter values, and the classification process continued with the most ideal segmentation result.

*2.2.3. Index-Based Class Extraction*

The spectral index types given in Table 2 were prepared with the B02, B03, B04, B07, B08, B11, and B12 bands with identical spatial resolutions (10 m) obtained by the downscaling process. These images have been used as a new layer containing a specific characteristic of the relevant class on the earth surface. Each spectral index is useful not only for estimating pixels with a specific property in land cover classification but also for improving accuracy of classification by combining it with other spectral index (Magpantay et al., 2019).

**Table 2.** *Environmental spectral indexes selected for OBIA*

| 9.5 | Name | Formulation | References |
|---|---|---|---|
| BAEI | Built-up area extraction index | (B4+0.3)/(B3+B11) | (Kebede et al., 2022) |
| BAI | Built-up area index | (B2-B8)/(B2+B8) | (Rahar & Pal, 2020) |
| BR28 | Band ratio 2/8 | B2/B8 | (Rouibah, 2023) |
| BR38 | Band ratio 3/8 | B3/B8 | (Rouibah, 2023) |
| MNDWI | M.N. difference water index | (B3-B11)/(B3+B11) | (Du et al., 2016) |
| NBAI | N. built-up area index | (B12-(B11/B3))/(B12+(B11/B3)) | (Li et al., 2021) |
| NBI | New built-up index | (B4*B12)/B8 | (Jieli et al., 2010) |
| NDVIre | N. difference red edge | (B7-B5)/(B7+B5) | (Osgouei et al., 2019) |
| NDTI | N. difference tillage index | (B11-B12)/(B11+B12) | (Osgouei et al., 2019) |
| NDVI | N. difference vegetation | (B8-B4)/(B8+B4) | (Wu et al., 2022) |
| NDWI | N. difference water index | (B3-B8)/(B3+B8) | (Zhang et al., 2019) |
| UI | Urban index | (B11-B8)/(B11+B8) | (Kebede et al., 2022) |

*All formulas are shown according to SENTINEL 2 MSI bands, M: Modified, N: Normalized*

The spectral reflectance value ranges that best represented the classes for six different land cover/land use classes (agriculture, pasture, built-up, water surfaces, forest, and bare land) were determined using the relevant index images. Given threshold values ranges (sub-top values) should not be considered as spectral information representing the entire class of interest on the image. The ranges where two different classes were thought to be mixed were not taken into consideration. At these points, the classification ability of the OBIA was used. In addition, DEM and Stand map were used to distinguish agriculture, pasture, and unhealthy forest cover, which have very similar spectral reflectance values, by considering the morphological structure of the study area. The obtained polygons were used as a training set to run the NN configuration process. After the configuration step, the accuracy assessment results were calculated using the up-to-date Google Earth images for the final classification layer. The entire process explained in the method section is shared on Figure 3, considering chronologically.

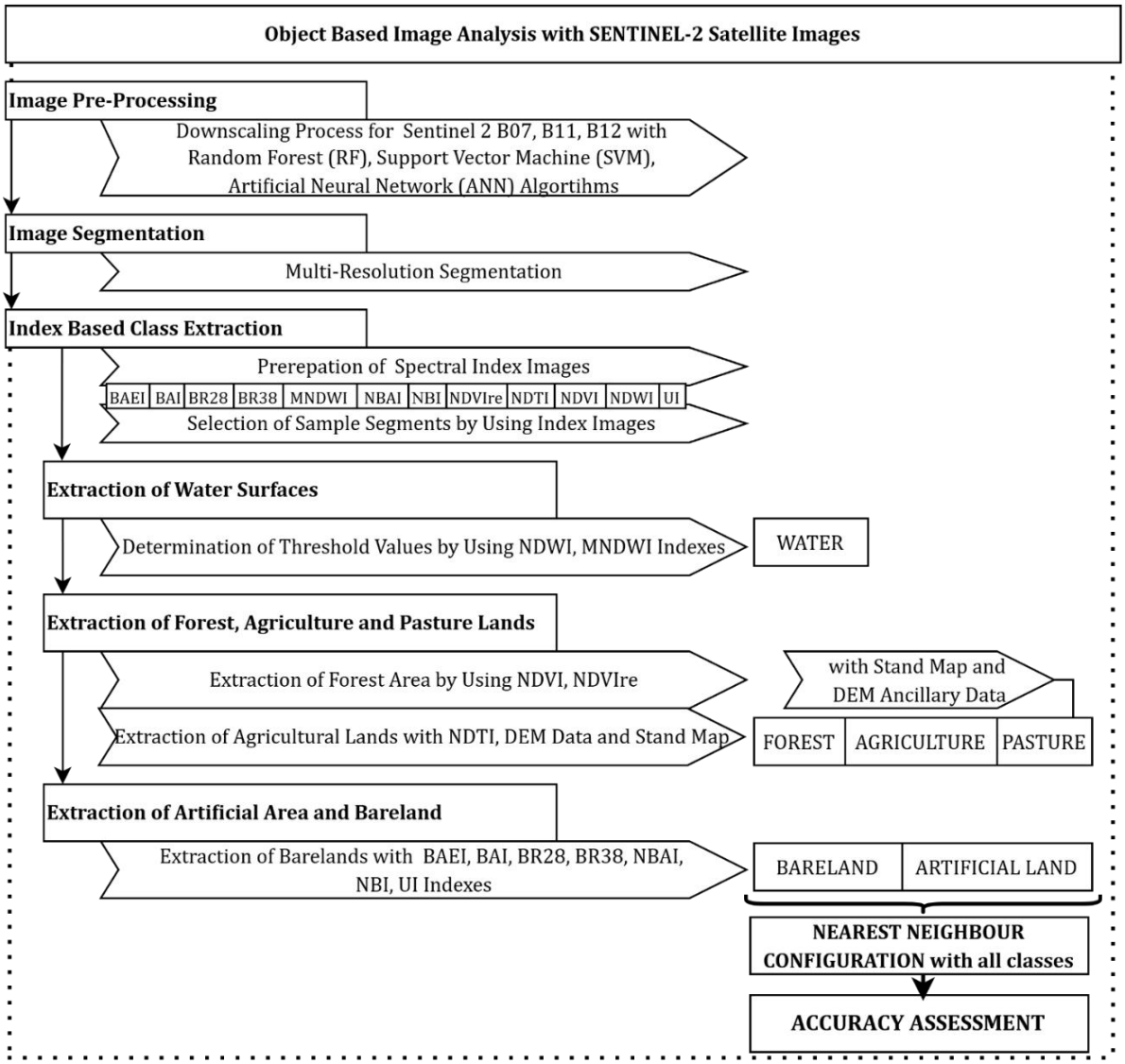


**Figure 3.** *Workflow of the object-based image classification based on spectral indexes*

## 3. RESULTS AND DISCUSSION

### 3.1. Results

#### *3.1.1. Image Downscaling Pre-Processing*

The variance inflation factor (VIF) of the data set was controlled to understand whether the multi-collinearity problem affects the model performance during the downscaling process. The VIF value for the entire data set was determined as 6.27. Since this value is below 10, the downscaling process of the B07, B11, and B12 bands was deemed appropriate by using the B02, B03, B04, and B08 bands. After this control step, B07, B11, and B12 bands with 20 m resolutions were subjected to downscaling process by running with B02, B03, B04, and B08 indicators. The interactive analysis of these models with the independent variable set enabled us to obtain solutions with different accuracy values using the same model and parameters. As a result of the experiments, the model with the highest accuracy was obtained with the Random Forest Algorithm for B07 and B11 bands with $R^2$ values of 0.95. The highest accuracy for the B12 band with $R^2$ values of 0.89 was obtained with ANN as seen in Table 3.

**Table 3.** *Image pre-processing downscaling results*

| Model | Target Band | Model Installation | RMSE | MAE | $R^2$ |
|---|---|---|---|---|---|
| SVM | B07 | Independent<br>B02, B03, B04, B08<br>SVM-Type:eps-regression<br>SVM-Kernel: radial<br>Gamma:0.25<br>Epsilon:0.1, Cost:1 | 279.35 | 212.05 | 0.89 |
| | B11 | | 221.72 | 181.03 | 0.88 |
| | B12 | | 235.44 | 199.96 | 0.84 |
| RF | **B07** | Cross Validation<br>Mtry:3<br>Method:cv<br>Number:5<br>Repeats:3<br>Search:grid | **296.87** | **227.91** | **0.95** |
| | **B11** | | **183.37** | **125.23** | **0.95** |
| | B12 | | 182.24 | 124.57 | 0.88 |
| ANN | B07 | with Normalized<br>Independent<br>B02, B03, B04, B08 | 279.35 | 212.05 | 0.89 |
| | B11 | | 188.21 | 200.98 | 0.91 |
| | **B12** | | **235.33** | **199.91** | **0.89** |

** Bold rows indicate the "best" performances for BO7, B11, B12 downscaling process*

### *3.1.2. Image Segmentation*

The segmentation process was repeated several times using different parameter values. As a result of the experiments, the parameter values that are best for separating the natural band composite image of the Silifke district into segments are presented in Table 4.

**Table 4.** *Parameter values used in the segmentation process*

| Segmentation Type | Shape | Compactness | Image Layer | Scale |
|---|---|---|---|---|
| multiresolution segmentation | 0.4 | 0.4 | 1.1.1.1.1.1.1. | 30 |

Using the parameter values shared in Table 4, the entire study area was divided into 26,544,659 segments. In here, two evaluations were needed to accept the segmentation result as valid. The first is that the object groups belonging to a class should be successfully separated from the other object groups. The second is that a class should not be subjected to unnecessary divisions within the object group belonging to its own class. Segmented images of the three different areas belonging to the study area is shown in Figure 4.

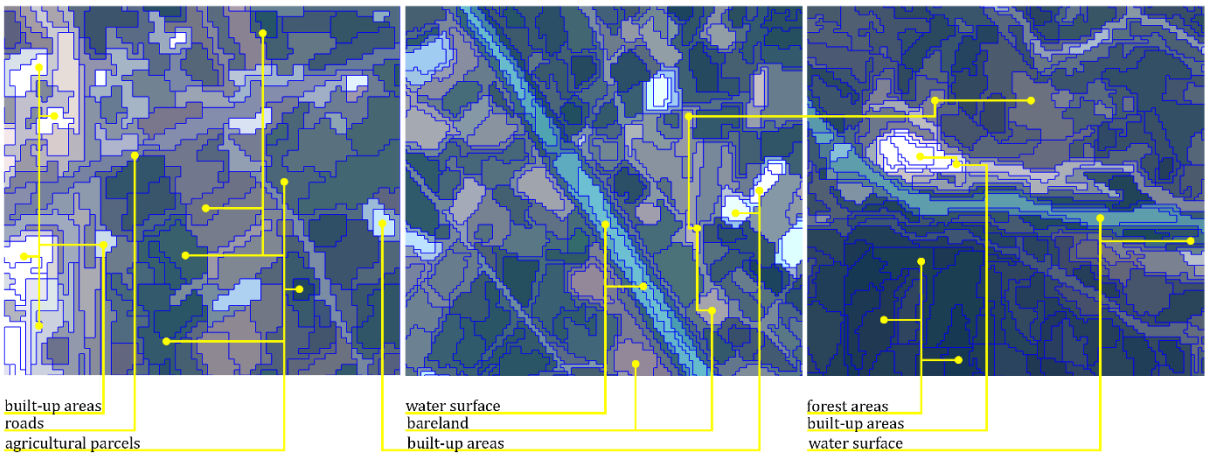


**Figure 4.** *Examples from the segmentation study performed*

### *3.1.2. Index Based Class Extraction*

Index layers were obtained using Sentinel 2 MSI bands B02, B03, B04, B05, B07, B08, B11, and B12 with identical spatial resolutions (10 m). This step was performed using the eCognition Developer 64 software. The layers (using formulations listed in Table 2) are shown in Figure 5.

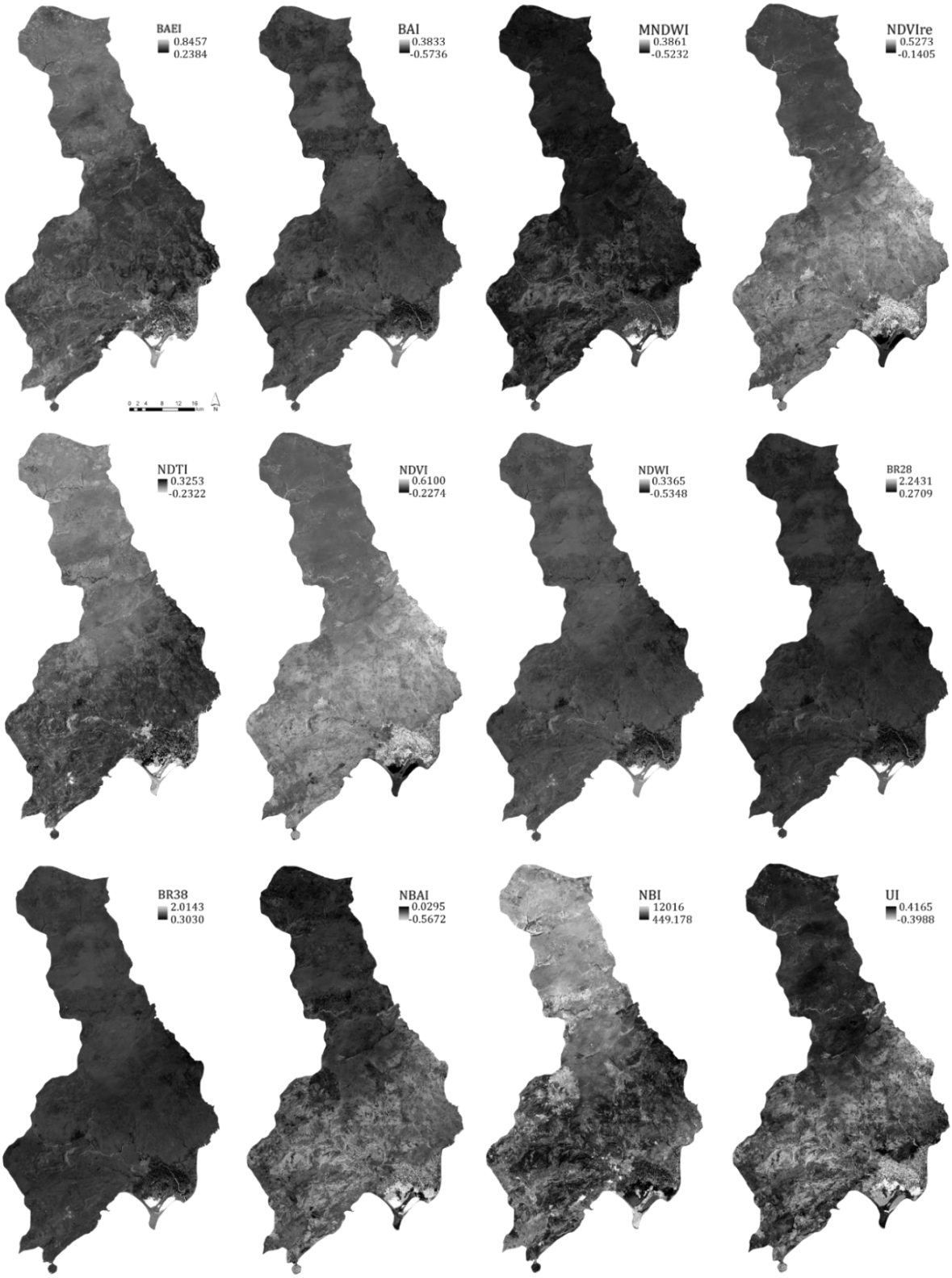


**Figure 5.** *Index layers created for OBIA using Sentinel 2 MSI bands*

Extracting all classes in a healthy way using the obtained index layers is not considered appropriate, especially for classes that provide similar spectral reflectance information, such as agriculture, forest, and pasture. For this reason, within the scope of this study, segments that clearly represent a total of six LC/LU classes were separated by utilizing the spectral information representing them (as seen in Table 5) and auxiliary data. It has been noticed that agricultural activities are concentrated in the lands with an altitude of 0-76 meters in Silifke district due to its morphological structure. These areas

were limited using DEM auxiliary data, and parcels belonging to agricultural activities were obtained using NDVI within this limited region. This method has been very effective in separating agricultural land from pasture and forest lands. In Türkiye, pasture activities are carried out on lands with high groundwater levels. This situation makes it difficult to distinguish pasture lands from shallow water surfaces and less dense or unhealthy forest lands. For this reason, pasture-land segments were extracted using the stand map.

**Table 5.** *Threshold values for class extraction*

| Name | Sub-value | Top-value | Used Ancillary Data | Related Class |
|---|---|---|---|---|
| NDWI | 0.0012 | 0.2802 | - | water |
| MNDWI | -0.0017 | 0.2931 | - | water |
| NDVI | 0.1 | 0.6100 | <76 m DEM | agriculture |
| NDVI | 0.22 | 0.6100 | >76 m DEM | forest |
| NDVIre | 0.1450 | 0.5273 | >76 m DEM | forest |
| NDTI | 0.0574 | 0.0976 | - | built-up |
| BAEI | 0.4423 | 0.5017 | after extracting water | built-up |
| BAI | -0.1922 | -0.0888 | after extracting forest | built-up |
| NDVI | 0.1203 | 0.1827 | via stand map | pasture |
| --- | - | - | after extracting all classes | bare land |
| BR28 | no meaningful class separation was obtained | | | |
| BR38 | | | | |
| NBAI | | | | |
| UI | | | | |
| NBI | | | | |

Another issue to be considered at this stage is the sequence of the class extraction steps. The sequence followed in this study is the same as the related class shared in Table 5. Inevitably, the minimum and maximum ranges of spectral reflectance values provided by remote sensing data within wide administrative boundaries such as Silifke district, would be large. This situation makes it difficult to distinguish between relevant classes. After each class extraction, removing the spectral range representing the class simplifies the process. In cases where more than one index was evaluated for the same class, all segments in the sub-value and top-value ranges were merged and included in the training set. For example, the extraction of segments belonging to the water class was obtained by merging polygons in the range of 0.0012 to 0.2802 for NDWI and -0.0017 to 0.2831 for MNDWI in the segmented image.

With BR28, BR38, NBAI, UI and NBI layers, meaningful information extraction was not achieved, and they were not used in the classification process. Except for these indexes, the polygons of the NDWI, MNDWI, NDVI, NDVIre, NDTI, BAEI and BAI, which allowed meaningful information extraction, were assigned to the relevant classes as training set. The obtained 10,328 polygons were used for the OBIA process covering the NN configuration. Thus, the classification process was completed. The final layer obtained after the classification process is shared in Figure 6.

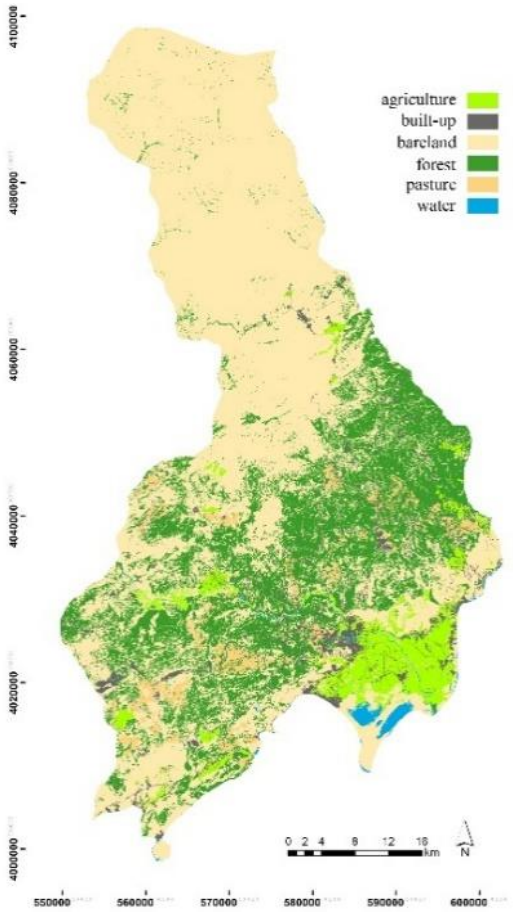


**Figure 6.** *Result classification layer*

*3.1.3. Accuracy Assessment*

To test the statistical accuracy of the classification, the valid Cochran's sample size was calculated as 119 (Woolson et al., 1986). The current ground-truth data consisting of 119 sample areas across all classes were compared with the classification results. The comparison outcomes were evaluated using producer and user accuracy metrics (Story & Congalton, 1986) and the kappa statistic (Congalton, 1991). The results of the accuracy assessment are presented in Table 6.

**Table 6.** *Accuracy assessment results*

| Class | Producer Accuracy | User Accuracy | Kappa Coefficient |
|---|---|---|---|
| Water | 1 | 1 | 0.8815 |
| Built-up | 0.7500 | 0.7500 | |
| Forest | 0.9333 | 0.9333 | |
| Agriculture | 0.6666 | 0.8571 | |
| Pasture | 1 | 1 | |
| Bare land | 0.9861 | 0.9594 | |
| **Overall Accuracy** | | | **0.9411** |

## 3.2. Discussion

When similar studies carried out using satellite images for the downscaling process were examined, it was observed that the models established with nonlinear machine learning algorithms (ANN, SVM, RF, Decision Tree (DT) etc.) produced quite successful results according to the model experiments established with linear ones (Lineer, Ridge, Lasso and Elastic Net Regression models etc.) (Gaitan et al., 2014; Ghorbanpour et al., 2021; Weichert & Bürger, 1998). In line with the relevant literature,

the downscaling model performances for bands B07, B11, and B12 were found to be statistically significant. Among nonlinear machine learning algorithms, the RF algorithm—recognized for its superior model performance (Grimm et al., 2008; Lamichhane et al., 2019; Reddy et al., 2024)—yielded the highest accuracy for the B07 and B11 bands in this study.

Although the BR28, BR38, NBAI, UI, and NBI have demonstrated significant results in numerous studies (Osgouei et al., 2019; Suharyadi et al., 2022; Xi et al., 2019), they failed to accurately extract the built-up class within the scope of this study, despite trials involving different spectral ranges. For instance, Rouibah (2023) concluded that the BR28 and BR38 were simple yet effective in distinguishing urban areas. However, the present study did not yield the same outcome. This discrepancy is largely attributable to the climatic differences between the study areas. While Rouibah (2023) conducted the research under arid climate conditions, the Silifke region is influenced by the Mediterranean climate. The impact of atmospheric conditions on spectral reflectance values is well documented (Kaufman, 1987). Therefore, differing results are to be expected.

Pandey & Tiwari (2020) used NBI and NBAI to extract roof surfaces and build-up areas in a small study area where construction was dense. However, the satellite image used in this study was AVIRIS-NG imagery hyperspectral data. AVIRIS-NG has 1999 $SWIR_{2,}$ 1548 $SWIR_{1,}$ 561 Green central wavelength combination (nm) for NBAI index, and 1999 $SWIR_{2,}$ 867 NIR, 737 Red central wavelength combinations (nm) for NBI index. However, Sentinel 2 MSI imagery has 2202 $SWIR_{2,}$ 1613 $SWIR_{1,}$ 559 Green central wavelengths combination (nm) for NBAI index, and 1613 $SWIR_{2,}$ 832 NIR, and 664 Red central wavelengths combination (nm). The spectral differences captured by the band sets also caused differences in the reflectance value distribution of the classes on the created NBAI and NBI images. According to the study area determined by Pandey & Tiwari (2020), the fact that the artificial surfaces (roof and other construction areas) in the Silifke district have a very heterogeneous distribution and the differences in the spectral reflectance values of the bands used caused different results in both studies.

Ali et al. (2022) successfully extracted city features using NDBI and UI. However, in their study, while NDBI played an active role in distinguishing the surfaces, UI showed effective performance for bare land and urban surfaces in the second step. Limiting the study to two classes contributed significantly to the result. The fact that the Silifke district did not have the same distribution density prevented similar results from being obtained. Öztürk (2022) aimed to extract impervious surfaces with UI index prepared using Sentinel-2a MSI and Landsat-9 OLI-2 satellite images but could not achieve a successful result as in this study. For this reason, built-up extraction attempts performed with the UI index could not be considered reliable.

The spectral range values found for the extraction of classes associated with the BAEI, BAI, MNDWI, NDVIre, NDTI, NDVI, and NDWI exhibit heterogeneity in various research regions, which is perfectly acceptable. These discrepancies could be caused by a variety of reasons, including the satellite platform's sun angle at the time of recording, bandwidth, receiver quality, and atmospheric conditions. For this reason, the quantitative results obtained (seen in Table 5) were not compared with similar studies.

Among the accuracy values obtained for the water, built-up, forest, agriculture, pasture, and bare land classes, the lowest value corresponds to agricultural areas, with a producer accuracy of 0.6666. According to Kappa Statistic introduced by Nichols et al. (2010), this value is accepted as "substantial agreement ($0.61<a<0.80$)" among the acceptable accuracy scores. As a result, every score from the classification research (shown in Table 6) is within an acceptable range. In the light of all this information, it is quite difficult to consider that the proposed method and threshold values reflect a standard. The method's use with different working areas and satellite image types necessitates testing with different threshold values. Therefore, obtaining effective results may require a sensitive

and long-term work process. This situation should not be ignored for research that will use a similar approach.

## 4. CONCLUSIONS

In studies based on estimation performance, such as downscaling with data provided through satellite platforms, the performance of nonlinear machine learning algorithms for the Silifke district and its surrounding areas is acceptable. The reliability of the obtained downscaled bands is essential for classification results of the indexes obtained. The object-based image classification process implemented in the study has proven that classification studies that can provide statistically acceptable accuracy scores are possible with spectral-based information layers. The results are consistent with similar studies, except for BR28, BR38, NBAI, UI, and NBI. The results proved the success of LC/LU classification with high-resolution Sentinel 2 MSI satellite images for the Silifke district located on the Mediterranean coast. This study presents an object-based image classification method that can be easily integrated into similar geographical areas using the spectral ranges (sub-top values) in Table 4. Correctly extracting classes with a high probability of mixing, such as low-density forest areas, agricultural areas, and pasture areas, is a quite difficult and time-consuming step for planners. The method presented in this study provides a solution to this problem for large study areas. OBIA (Tonbul & Kavzoğlu, 2018), which does not only consider the reflection information in pixels, has proven its classification success in large study areas, as in this study. The potential of OBIA on spectrally complex images has enabled the development of a method that simplifies the ensuing process by following processing steps. The Silifke district has a very heterogeneous LC/LU distribution. Therefore, it is complex to convert the spectral diversity into information. In similar purpose studies conducted by considering spectral index layers as a reference, the sample areas are quite small. Researchers present the success of the indexes by testing in these small study areas. These studies are quite meaningful, but they are not sufficient to carry out classification studies that can ensure the readability of lands at the planning level. In this study, the deficiency has been eliminated with the help of auxiliary data that can be easily integrated into the OBIA process.

Beyond methodological validation, this study provides a practical and scalable classification approach that can be used by local governments and researchers in areas such as rural and regional planning, ecosystem monitoring, and environmental impact assessment. The ability to correctly classify classes with a high probability of mixing contributes to more sustainable spatial planning decisions.

### *Author Declarations and CRediT Roles*

There is no conflict of interest. No financial support has been received. Ethical committee approval is not required. Generative artificial intelligence tools have not been used. It has not been previously presented or published. Data will be made available upon request.

Conceptualization: EK; Data curation: EK; Formal analysis: EK, ÖFU; Investigation: EK, ÖFU; Methodology: EK; Resources: EK, ÖFU; Software: EK; Supervision: EK; Validation: EK; Visualization: EK; Writing – original draft: EK, ÖFU; Writing – review & editing: ÖFU.

## REFERENCES

Ali, U., Esau, T. J., Farooque, A. A., Zaman, Q. U., Abbas, F., & Bilodeau, M. F. (2022). Limiting the collection of ground truth data for land use and land cover maps with machine learning algorithms. *ISPRS International Journal of Geo-Information*, *11*(6), 333. https://doi.org/10.3390/ijgi11060333

Bayburt, S. (2009). *Uydu görüntülerinin piksel ve nesne tabanlı sınıflandırma sonuçlarının karşılaştırılması (Doğu Trakya bölgesi örneği)* (Thesis no. 251917) [Master's thesis, İstanbul Technical University]. Council of Higher Education Thesis Center.

Bhaskaran, S., Paramananda, S., & Ramnarayan, M. (2010). Per-pixel and object-oriented classification methods for mapping urban features using Ikonos satellite data. *Applied Geography, 30*, 650–665. https://doi.org/10.1016/j.apgeog.2010.01.009

Bhatt, A., Ghosh, S. K., & Kumar, A. (2018). Spectral indices based object oriented classification for change detection using satellite data. *International Journal of System Assurance Engineering and Management, 9*, 33–42. https://doi.org/10.1007/s13198-016-0458-7

Blaschke, T. (2010). Object based image analysis for remote sensing. *ISPRS Journal of Photogrammetry and Remote Sensing, 65*(1), 2–16. https://doi.org/10.1016/j.isprsjprs.2009.06.004

Congalton, R. G. (1991). A review of assessing the accuracy of classifications of remotely sensed data. *Remote Sensing of Environment, 37*(1), 35–46. https://doi.org/10.1016/0034-4257(91)90048-B

Copernicus Browser (CB). (2024, March 1). *Data sources: SENTINEL-2*. https://browser.dataspace.copernicus.eu/

Da Silva, V. S., Salami, G., Da Silva, M. I. O., Silva, E. A., Junior, J. J. M., & Alba, E. (2020). Methodological evaluation of vegetation indexes in land use and land cover (LULC) classification. *Geology, Ecology, and Landscapes, 4*(2), 159–169. https://doi.org/qg99

Du, Y., Zhang, Y., Ling, F., Wang, Q., Li, W., & Li, X. (2016). Water bodies' mapping from Sentinel-2 imagery with modified normalized difference water index at 10-m spatial resolution produced by sharpening the SWIR band. *Remote Sensing*, *8*(4), 354. https://doi.org/10.3390/rs8040354

Duro, D. C., Franklin, S. E., & Dubé, M. G. (2012). A comparison of pixel-based and object-based image analysis with selected machine learning algorithms for the classification of agricultural landscapes using SPOT-5 HRG imagery. *Remote Sensing of Environment, 118*, 259–272. https://doi.org/10.1016/j.rse.2011.11.020

Esetlili, M. T., Balcık, F. B., Şanlı, F. B., Üstüner, M., Kalkan, K., Göksel, Ç., Gazioğlu, C., & Kurucu, Y. (2018). Comparison of object and pixel-based classifications for mapping crops using RapidEye imagery: A case study of Menemen Plain, Turkey. *International Journal of Environment and Geoinformatics (IJEGEO), 5*(2), 231–243. https://doi.org/10.30897/ijegeo.442002

Flanders, D., Hall-Beyer, M., & Pereverzoff, J. (2003). Preliminary evaluation of eCognition object-based software for cut block delineation and feature extraction. *Canadian Journal of Remote Sensing, 29*(4), 441–452. https://doi.org/10.5589/m03-006

Gaitan, C. F., Hsieh, W. W., Cannon, A. J., & Gachon, P. (2014). Evaluation of linear and non-linear downscaling methods in terms of daily variability and climate indices: surface temperature in Southern Ontario and Quebec, Canada. *Atmosphere-Ocean, 52*(3), 211–221. https://doi.org/10.1080/07055900.2013.857639

Ghorbanpour, A. K., Hessels, T., Moghim, S., & Afshar, A. (2021). Comparison and assessment of spatial downscaling methods for enhancing the accuracy of satellite-based precipitation over Lake Urmia Basin. *Journal of Hydrology*, *596*, 126055. https://doi.org/10.1016/j.jhydrol.2021.126055

Grimm, R., Behrens, T., Märker, M., & Elsenbeer, H. (2008). Soil organic carbon concentrations and stocks on Barro Colorado Island - Digital soil mapping using Random Forests analysis. *Geoderma, 146*(1–2), 102–113. https://doi.org/10.1016/j.geoderma.2008.05.008

Harrak, Y., Rachid, A., & Aguejdad, R. (2025). Evaluation of spectral indices and global thresholding methods for the automatic extraction of built-up areas: An application to a semi-arid climate using Landsat 8 imagery. *Urban Science*, *9*(3), 78. https://doi.org/10.3390/urbansci9030078

Hong, S.-H., Hendrickx, J. M. H., & Borchers, B. (2011). Down-scaling of SEBAL derived evapotranspiration maps from MODIS (250 m) to Landsat (30 m) scales. *International Journal of Remote Sensing, 32*(21), 645–6477. https://doi.org/10.1080/01431161.2010.512929

Jawak, S. D., Devliyal, P., & Luis, A. J. (2015). A comprehensive review on pixel oriented and object oriented methods for information extraction from remotely sensed satellite images with a special emphasis on cryospheric applications. *Advances in Remote Sensing, 4*(3), 177–195. https://doi.org/10.4236/ars.2015.43015

Jieli, C., Manchun, L., Yongxue, L., Chenglei, S., & Wei, H. (2010). Extract residential areas automatically by new built-up index. In *2010 18th International Conference on Geoinformatics* (Vol. 3, pp. 171–175). IEEE. https://doi.org/10.1109/GEOINFORMATICS.2010.5567823

Kalkan, K., & Maktav, D. (2010). Comparison of object-based and pixel-based classification methods. In T. Kavzaoğlu & D. Maktav (Eds.), *III. remote sensing and geographic information systems symposium* (pp. 153–160).

Karakus, P., Karabork, H., & Kaya, S. (2017). A comparison of the classification accuracies in determining the land cover of Kadirli Region of Turkey by using the pixel based and object based classification algorithms. *International Journal of Engineering and Geosciences (IJEG), 2*(2), 52–60.

Kaufman, Y. J. (1987). Atmospheric effect on spectral signature – measurements. *Advances in Space Research, 7*(11), 203–206. https://doi.org/10.1016/0273-1177(87)90313-9

Kawamura, M., Jayamanna, S., & Tsujiko, Y. (1996). Relation between social and environmental conditions in Colombo Sri Lanka and the urban index estimated by satellite remote sensing data. *International Archives of Photogrammetry and Remote Sensing, 31*, 321–326.

Kebede, T. A., Hailu, B. T., & Suryabhagavan, K. V. (2022). Evaluation of spectral built-up indices for impervious surface extraction using Sentinel-2A MSI imageries: A case of Addis Ababa city, Ethiopia. *Environmental Challenges, 8*, 100568. https://doi.org/10.1016/j.envc.2022.100568

Lamichhane, S., Kumar, L., & Wilson, B. (2019). Digital soil mapping algorithms and covariates for soil organic carbon mapping and their implications: A review. *Geoderma, 352*, 395–413. https://doi.org/10.1016/j.geoderma.2019.05.031

Lemenkova, P., & Debeir, O. (2023). Computing vegetation indices from the satellite images using GRASS GIS scripts for monitoring mangrove forests in the coastal landscapes of Niger Delta, Nigeria. *Journal of Marine Science and Engineering*, *11*(4), 871. https://doi.org/10.3390/jmse11040871

Li, C., Shao, Z., Zhang, L., Huang, X., & Zhang, M. (2021). A comparative analysis of index-based methods for impervious surface mapping using multiseasonal Sentinel-2 satellite data. *IEEE Journal of Selected Topics in Applied Earth Observations and Remote Sensing, 14*, 3682–3694. https://doi.org/10.1109/jstars.2021.3067325

Magpantay, A. T., Adao, R. T., Bombasi, J. L., Lagman, A. C., Malasaga, E. V., & Ye, C.-S. (2019). Analysis on the effect of spectral index images on improvement of classification accuracy of Landsat-8 OLI image. *Korean Journal of Remote Sensing, 35*(4), 561–571. https://doi.org/10.7780/kjrs.2019.35.4.6

McFeeters, S. K. (1996). The use of the Normalized Difference Water Index (NDWI) in the delineation of open water features. *International Journal of Remote Sensing, 17*(7), 1425–1432. https://doi.org/10.1080/01431169608948714

Myint, S. W., Gober, P., Brazel, A., Grossman-Clarke, S., & Weng, Q. (2011). Per-pixel vs. object-based classification of urban land cover extraction using high spatial resolution imagery. *Remote Sensing of Environment, 115*(5), 1145–1161. https://doi.org/10.1016/j.rse.2010.12.017

Nandam, V., & Patel, P. L. (2021). A novel hybrid approach using SVM and spectral indices for enhanced land use land cover mapping of coastal urban plains. *Geocarto International, 37*(16), 4714–4736. https://doi.org/10.1080/10106049.2021.1899300

NASA (2025, February 26). *Earth data Sentinel-2 MSI*. https://tinyurl.com/4dacb7ar

Newman, M. E., McLaren, K. P., & Wilson, B. S. (2011). Comparing the effects of classification techniques on landscape-level assessments: pixel-based versus object-based classification. *International Journal of Remote Sensing, 32*(14), 4055–4073. https://doi.org/10.1080/01431161.2010.484432

Nichols, T. R., Wisner, P. M., Cripe, G., & Gulabchand, L. (2010). Putting the kappa statistic to use. *The Quality Assurance Journal, 3*(3–4), 41–77. https://doi.org/10.1002/qaj.481

Nussbaum, S., & Menz, G. (2008). *eCognition image analysis software*. In T. Blaschke, S. Lang, & G. J. Hay (Eds.), *Object-based image analysis and treaty verification* (pp. 129–143). Springer. https://doi.org/10.1007/978-1-4020-6961-1_3

Nwagoum, C. S. K., Yemefack, M., Tedou, F. B. S., & Oben, F. T. (2023). Sentinel-2 and Landsat-8 potentials for high-resolution mapping of the shifting agricultural landscape mosaic systems of southern Cameroon. *International Journal of Applied Earth Observation and Geoinformation*, *124*, 103545. https://doi.org/10.1016/j.jag.2023.103545

Orman Genel Müdürlüğü. (OGM). (2021). *E-harita uygulamasi- Meşçere*. https://cbs.ogm.gov.tr/vatandas/

Osgouei, P. E., Kaya, S., Sertel, E., & Alganci, U. (2019). Separating built-up areas from bare land in mediterranean cities using sentinel-2A imagery. *Remote Sensing, 11*, 345. https://doi.org/10.3390/rs11030345

Ouchra, H., Belangour, A., & Erraissi, A. (2022). A comparative study on pixel-based classification and object-oriented classification of satellite image. *International Journal of Engineering Trends and Technology, 70*(8), 206–215. https://doi.org/10.14445/22315381/ijett-v70i8p221

Özgür, D. (2023, March 3). *Coğrafi bilgi sistemleri verileri, Türkiye sayısallaştırılmış yükselti modeli (dijital yükseklik modeli (DEM))*. https://www.ozgurcografya.com/

Öztürk, D. (2022). Sentinel-2A MSI ve Landsat-9 OLI-2 görüntüleri kullanılarak farklı geçirimsiz yüzey indekslerinin karşılaştırmalı değerlendirmesi: Samsun örneği. *Ege Coğrafya Dergisi, 31*(2), 401–423. https://doi.org/10.51800/ecd.1175827

Pandey, D., & Tiwari, K. C. (2020). Extraction of urban built-up surfaces and its subclasses using existing built-up indices with separability analysis of spectrally mixed classes in AVIRIS-NG imagery. *Advances in Space Research, 66*(8), 1829–1845. https://doi.org/10.1016/j.asr.2020.06.038

Rahar, P. S., & Pal, M. (2020). Comparison of various indices to differentiate built-up and bare soil with Sentinel 2 Data. In J. K. Ghosh & I. da Silva (Eds.), *Applications of geomatics in civil engineering* (pp. 501–509). Springer. https://doi.org/10.1007/978-981-13-7067-0_39

Rastner, P., Bolch, T., Notarnicola, C., & Paul, F. (2014). A comparison of pixel- and object-based glacier classification with optical satellite images. *IEEE Journal of Selected Topics in Applied Earth Observations and Remote Sensing, 7*(3), 853–862. https://doi.org/10.1109/jstars.2013.2274668

Reddy, B. B. K., Maragatham, S., Santhi, R., Balachandar, D., Vijayalakshmi, D., Vasu, D., & Gopalakrishnan, M. (2024). Predictive soil mapping using random forest models: Applications in pH and soil organic matter assessment. *Plant Science Today, 11*(4), 1–12. https://doi.org/10.14719/pst.3865

Rouibah, K. (2023). The use of bands ratio derived from Sentinel-2 imagery to detect built-up area in the dry period (North-East Algeria). *Applied Geomatics, 15*, 473–482. https://doi.org/10.1007/s12518-023-00513-y

Rouse, J. W., Haas, R. H., Schell, J. A., & Deering, D. W. (1973). Monitoring vegetation systems in the great plains with ERTS [Symposium paper]. In S. C. Freden & E. P. Mercanti (Eds.), *Proceedings of the third earth resources technology satellite-1 symposium* (pp. 309–317).

Sentiwiki. (2025, March 26). *Sentinel-2 products MSI products overview*. https://sentiwiki.copernicus.eu/web/s2-products

Story, M., & Congalton, R. G. (1986). Accuracy assessment: a user's perspective. *Photogrammetric Engineering and Remote Sensing, 52*(3), 397–399.

Suharyadi, R., Umarhadi, D. A., Awanda, D., & Widyatmanti, W. (2022). Exploring built-up indices and machine learning regressions for multi-temporal building density monitoring based on Landsat series. *Sensors, 22*, 4716. https://doi.org/10.3390/s22134716

Tehrany, M. S., Pradhan, B., & Jebuv, M. N. (2014). A comparative assessment between object and pixel-based classification approaches for land use/land cover mapping using SPOT 5 imagery. *Geocarto International, 29*(4), 351–369. https://doi.org/10.1080/10106049.2013.768300

Tonbul, H., & Kavzoğlu, T. (2018). Nesne tabanli görüntü analizinde görüntü bölütleme yaklaşimlari ve bölütleme kalitesinin analizi. *Harita Dergisi, 160*, 12–23. https://doi.org/10.15659/uzalcbs2018.6403

Torres-Sanchez, J., Lopez-Granados, F., & Pena, J. M. (2015). An automatic object-based method for optimal thresholding in UAV images: Application for vegetation detection in herbaceous crops. *Computers and Electronics in Agriculture, 114*, 43–52. https://doi.org/f7jhbp

Trimble. (2025, March 26). *eCognition suite documentation*. https://docs.ecognition.com

TÜİK (2023, April 12). *İl ve ilçe merkezlerine göre nüfus ve yüzölçümü verileri*. https://bit.ly/4pw7Dh2

Weichert, A., & Bürger, G. (1998). Linear versus nonlinear techniques in downscaling. *Climate Research, 10*, 83–93. https://doi.org/10.3354/cr010083

Whiteside, T. G., Boggs, G. S., & Maier, S. W. (2011). Comparing object-based and pixel-based classifications for mapping savannas. *International Journal of Applied Earth Observation and Geoinformation, 13*(6), 884–893. https://doi.org/10.1016/j.jag.2011.06.008

Woolson, R. F., Bean, J. A., & Rojas, P. B. (1986). Sample size for case-control studies using Cochran's statistic. *Biometrics, 42*(4), 927–932. https://doi.org/10.2307/2530706

Wu, B., Zheng, H., Xu, Z., Wu, Z., & Zhao, Y. (2022). Forest burned area detection using a novel spectral index based on multi-objective optimization. *Forests, 13*(11), 1787–1807. https://doi.org/10.3390/f13111787

Xi, Y., Thinh, N. X., & Li, C. (2019). Preliminary comparative assessment of various spectral indices for built-up land derived from Landsat-8 OLI and Sentinel-2A MSI imageries. *European Journal of Remote Sensing, 52*(1), 240–252. https://doi.org/10.1080/22797254.2019.1584737

Zha, Y., Gao, J., & Ni, S. (2003). Use of normalized difference built-up index in automatically mapping urban areas from TM imagery. *International Journal of Remote Sensing, 24*(3), 583–594. https://doi.org/10.1080/01431160304987

Zhang, K., Chen, Y., Wang, W., Wu, Y., Wang, B., & Yan, Y. (2023). A method for remote sensing image classification by combining Pixel Neighbourhood Similarity and optimal feature combination. *Geocarto International, 38*, 2158948. https://doi.org/10.1080/10106049.2022.2158948

Zhang, T.-X., Su, J.-Y., Liu, C.-J., & Chen, W.-H. (2019). Potential Bands of Sentinel-2A Satellite for Classification Problems in Precision Agriculture. *International Journal of Automation and Computing, 16*(1), 16–26. https://doi.org/10.1007/s11633-018-1143-x